

---

---

# Vibroacoustic Analysis and Response Suppression of a Rectangular Sandwich Electrorheological Panel

Seyyed M. Hasheminejad, S. M. Parvasi and A. Fadavi-Ardakani

*Acoustics Research Laboratory, Center of Excellence in Experimental Solid Mechanics and Dynamics, School of Mechanical Engineering, Iran University of Science and Technology, Narmak, Tehran 16844 Iran*

(Received 19 February 2014; accepted 17 January 2015)

A modal summation method based on far-field sound intensity is used to study the average radiation efficiency and the corresponding radiation power of a point-excited, simply-supported, rectangular sandwich plate containing a tunable electrorheological fluid (ERF) core, and set in an infinite rigid baffle. In addition, a classical analytical procedure based on the Rayleigh integral equation method is adopted to investigate the sound transmission characteristics (TL) of the adaptive plate insonified by plane pressure waves at an arbitrary angle of incidence, or excited by a perfectly diffuse sound field with a Gaussian directional distribution of energy. Numerical results reveal the imperative influence of an applied electric field strength (0–3.5 kV/mm) on controlling acoustic radiation from (or sound transmission through) the smart panel in a wide frequency range. In addition, an effort is made to find the optimal electric field which yields improved sound radiation and transmission characteristics for each excitation frequency. Limiting cases are considered and good agreements with the solutions available in the literature used in this study are obtained.

---

## 1. INTRODUCTION

Plates are one of the most extensively used structural components in industrial applications. Many civil, industrial, and modern aerospace and aeronautical structures (*e.g.*, walls and floors, ship hulls, machine elements, and aircraft sidewalls) can be practically modelled, to a first approximation, as a finite baffled panel. Throughout the past few decades, vibroacoustic problems involving acoustic radiation from (or sound transmission through) finitely bounded isolated panel structures have been subject to intense research. In particular, numerous efforts have been concentrated on studying the sound radiation and transmission characteristics of rectangular plates with various complications since early 1960s.<sup>1</sup> Maidanik<sup>2</sup> was the first to apply the concept of power flow and statistical energy analysis to derive several approximate asymptotic expressions for calculating the modal radiation resistance in different wavenumber regions for a simply-supported, rectangular isotropic plate placed in an otherwise rigid co-planar baffle. Wallace<sup>3</sup> subsequently used the Rayleigh integral to derive analytical expressions for the modal radiation efficiency of a simply-supported baffled rectangular panel. Leppington, *et al.*<sup>4</sup> provided a detailed mathematical analysis of the modal radiation from a simply-supported panel, and used the assumption of high modal densities to revise some of Maidanik's results for large acoustic wavenumbers, especially in the ranges close to the critical frequency.

Roussos<sup>5</sup> developed an analytical procedure for an efficient solution of sound transmission through a rectangular, simply-supported, isotropic or symmetrically laminated composite plate in an infinite rigid baffle and under arbitrary plane wave incidence. Panneton and Atalla<sup>6</sup> used a three-dimensional finite element model coupled with a boundary element approach to predict the sound transmission loss through multi-layer structures made of elastic, acoustic, and poroelastic (Biot) media. Lee and Kondo<sup>7</sup> presented analytical and exper-

imental studies of noise transmission loss of a three-layered simply-supported baffled rectangular plate with a viscoelastic core. Foin, *et al.*<sup>8</sup> proposed a variational model to analyse the vibroacoustic behaviour of a rectangular, baffled, simply-supported plate covered by a free or a constrained viscoelastic layer and immersed in either a light or a heavy fluid. Foin, *et al.*<sup>9</sup> investigated the vibroacoustic behaviour of an elastic, simply-supported rectangular plate covered by a locally reacting decoupling layer immersed in water and subjected to a point force disturbance. Sgard, *et al.*<sup>10</sup> employed the finite element method to predict sound-transmission loss across finite-sized, double-panel sound barrier with poroelastic linings. Berry, *et al.*<sup>11</sup> investigated the vibroacoustic response of a finite, simply-supported rectangular plate covered by a thick layer of decoupling material and immersed in a heavy fluid. Park, *et al.*<sup>12</sup> used the Rayleigh-Ritz method to investigate the effects of the support properties (stiffness and damping) on the forced vibration response and the associated radiated sound of viscoelastically supported rectangular plates.

Chiello, *et al.*<sup>13</sup> used a free-interface component mode synthesis technique associated with the finite element method to study the vibroacoustic behaviour of an elastically-supported baffled plate excited by a plane wave or a diffuse field. Xie, *et al.*<sup>14</sup> used results from a modal summation method based on the farfield sound intensity to investigate the average radiation efficiency of point-excited baffled rectangular plates, including those with a very large aspect ratio (strips). Au and Wang<sup>15</sup> investigated sound radiation from forced vibration of rectangular orthotropic plates with general boundary conditions traversed by moving loads. Park and Mongeau<sup>16</sup> used the Mindlin plate theory and the Rayleigh-Ritz method to investigate the vibroacoustic characteristics of sandwich panels with viscoelastic supports. Assaf and Guerich<sup>17</sup> used a finite element formulation coupled to a boundary element method to predict noise transmission loss (TL) through viscoelastically-damped sandwich rectangular plates subjected to an acoustic plane wave or

a diffuse sound field excitation.

Chazot and Guyader<sup>18</sup> used the so-called patch-mobility method to predict vibroacoustic behaviour of (or sound transmission through) double panels filled with poroelastic materials. Assaf, *et al.*<sup>19</sup> presented a finite element formulation to analyse the vibroacoustic response of plates with a constrained-layer damping treatment immersed in a light or heavy fluid. Zhou and Crocker<sup>20</sup> used two different boundary element analyses to investigate the sound transmission characteristics of foam-filled honeycomb sandwich panels excited by a random incidence acoustic field. Loredó, *et al.*<sup>21</sup> used Rayleigh–Ritz’s method for vibroacoustic analysis of baffled rectangular plates with constrained-layer damping (viscoelastic) patches. Li<sup>21</sup> studied active modal control of the vibroacoustic response of a fluid-loaded baffled rectangular plate using piezoelectric actuators and sensors and negative velocity feedback. He showed that the proposed method increases the modal damping ratio of the controlled mode and achieves notable reductions in the associated sound power and mean square velocity. Just recently, Kam, *et al.*<sup>23</sup> presented a semi-analytical approach based on the Rayleigh–Ritz method and the first Rayleigh integral for vibroacoustic analysis of elastically-restrained shear deformable stiffened rectangular orthotropic plates, and validated their results by carrying out experiments.

Vibration and sound radiation and transmission control of elastic structures is a crucial issue in many engineering systems, ranging from ground-based vehicles to machinery, civil structures, ships, aircrafts, aerospace vehicles, space-based platforms, and buildings. Two different approaches are normally used - passive control and active control. In the passive control approach, the material properties of the structure itself, such as damping and stiffness, are customized so as to modify the structural response. However, the material properties of such structures are preset in their design or construction stage, which can hardly be adapted to unanticipated environmental variations. Over the past few decades, intelligent materials such as piezoelectric materials, shape memory alloys, or electro- or magneto-rheological materials have been incorporated into conventional structures in order to adjust to the changes of the environment.<sup>24,25</sup> The latter materials have recently gained increasing recognition, as their rheological properties (damping and stiffness) can swiftly and reversibly be varied when subjected to an electrical field.<sup>26</sup>

Other valuable features of these materials include simplicity, compactness, low cost, low-energy loss, robustness, and easy controllability by computers,<sup>27</sup> which makes them an ideal methodology for noise and vibration control in various spheres of engineering. Consequently, numerous investigators have thoroughly studied the use of smart electro- or magneto-rheological-based structures for vibration control in various spheres of engineering.<sup>28–32</sup> There are, however, comparatively fewer authors who have investigated the sound radiation and insulation characteristics of these structures. Among them, Choi, *et al.*<sup>33</sup> formulated a fuzzy control logic on the basis of field-dependent sound pressure levels to experimentally investigate noise control of a rectangular closed cabin featuring one side of an ER fluid-based smart plate. Szary<sup>34</sup> examined the sound transmission loss for various kinds of electrorheological suspensions placed between two specially designed barriers under a variable alternative electric field den-

sity in a frequency range from 100 Hz to 2 kHz. Lu, *et al.*<sup>35</sup> experimentally studied the dynamic and acoustic characteristics of a sandwich cylindrical shell structure with an electrorheological fluid core, excited by an internal high frequency noise source. In a series of experimental investigations, Tang, *et al.*<sup>36</sup> devised sandwiched flexible electrorheological gel layers and studied the tunable behaviour of the transmitted sound-pressure levels with respect to the external electric field. More recently, Hasheminejad and Shabanimotlagh<sup>37</sup> employed the linear theory of elasticity in conjunction with the classical structural damping model, involving complex-valued field-dependent material constants, to develop a two-dimensional analytic solution for sound transmission control through an MRE-based adaptive sandwich infinite panel of arbitrary thickness.

The above review indicates that while there exists a notable body of literature on vibroacoustic characteristics of composite panels, rigorous analytical or numerical solutions for the sound radiation or transmission characteristics of finitely-bounded ERF-based sandwich structures seems to be absent. Thus, in this paper, we employ the equations of motion for a simply-supported ERF-filled rectangular sandwich plate,<sup>38</sup> the classical complex modulus approach for describing the viscoelastic behaviour of the ER core fluid,<sup>31</sup> the pertinent wave field expansions, and the modal summation method<sup>14</sup> along with the Rayleigh integral equation approach<sup>1</sup> to fill this gap. The proposed model is of noble interest, largely due to its inherent value as a canonical problem in structural acoustics. It can lead to further understanding of the acoustic behaviour of ER-material-based adaptive structures. It is also of practical value for noise control engineers involved in the development of reliable analytical and/or experimental tools for the design and analysis of ERF-based plates or panels with optimal acoustical characteristics.<sup>33–37</sup> Lastly, the presented analytical solution can serve as the benchmark for a comparison to solutions obtained by strictly numerical or asymptotic approaches.

## 2. FORMULATION

### 2.1. Governing Equations for the ERF Plate

The problem configuration is shown in Fig. 1. A sandwich rectangular plate ( $a \times b$ ) consisting of a base plate (thickness  $h_3$ ), a constraining layer (thickness  $h_1$ ), and a tunable fluid core layer (thickness  $h_2$ ), with simply-supported edge conditions, is considered. The skin layers are assumed to be cross-ply elastic composite laminates, with no slipping with respect to the core layer, and where identical transverse displacements are assumed at every point across the cross section for all three layers  $w(x, y, t)$ . Using Hamilton’s principle, after some tedious manipulations, the displacement equations of motion for the ERF-sandwich plate can readily be obtained, as outlined in details in the work of Hasheminejad and Maleki.<sup>38</sup> To consider the steady state vibrational response of the simply-supported adaptive plate, one may advantageously assume a harmonic normal resultant force acting on the upper surface of the plate (e.g., see Fig. 1(a)) which, along with the relevant displacement components, can be expanded in double Fourier series

as<sup>39</sup>

$$\begin{aligned}
 q(x, y, t) &= \\
 q_0(x, y)e^{i\omega t} &= \sum_{m=1}^{\infty} \sum_{n=1}^{\infty} q_{mn} \sin(\alpha_m x) \sin(\beta_n y) e^{i\omega t}; \\
 u_i(x, y, t) &= \sum_{m=1}^{\infty} \sum_{n=1}^{\infty} U_{mn}^{(i)} \cos(\alpha_m x) \sin(\beta_n y) e^{i\omega t}; \\
 v_i(x, y, t) &= \sum_{m=1}^{\infty} \sum_{n=1}^{\infty} V_{mn}^{(i)} \sin(\alpha_m x) \cos(\beta_n y) e^{i\omega t}; \\
 w(x, y, t) &= \sum_{m=1}^{\infty} \sum_{n=1}^{\infty} W_{mn} \sin(\alpha_m x) \sin(\beta_n y) e^{i\omega t}; \quad (1)
 \end{aligned}$$

where  $\omega$  is the excitation frequency,  $\alpha_m = m\pi/a$ ,  $\beta_n = n\pi/b$ ,  $u_i$  and  $v_i$  ( $i = 1, 3$ ) are the mid-plane deformations of the skin layers in the  $x$  and  $y$  directions, respectively,  $U_{mn}^{(i)}$ ,  $V_{mn}^{(i)}$  ( $i = 1, 3$ ) and  $W_{mn}$  are unknown modal coefficients, and  $q_{mn} = \frac{4}{ab} \int_0^b \int_0^a q_0(x, y) \sin(\alpha_m x) \sin(\beta_n y) dx dy$  ( $m, n = 1, 2, 3, \dots$ ) are the Fourier coefficients associated with the harmonic distributed normal force of amplitude  $q_0(x, y)$ . By direct substitution of the displacement expansions in Eq. (1) into the governing equations of motion for the ERF plate (see Eq. 19 in Hasheminejad's and Maleki's work<sup>38</sup>), after some manipulations, one obtains (2) (see the top of the next page), where  $i = 1, 3$ ;  $\delta_i = 1$  if  $i = 1$ ; and  $\delta_i = 1$  if  $i = 3$ ,  $\rho_i$  ( $i = 1, 2, 3$ ) denotes the mass density in the  $i$ -th layer;  $I_2 = (\rho_2 h_2^3 / 12)$  is the mass moment of inertia of the ER fluid interlayer;  $G^{(2)}$  is the viscoelastic shear modulus of the ER fluid layer;  $d = h_1/2 + h_2 + h_3/2$ ; and  $(A_{jk}^{(i)}, B_{jk}^{(i)}, D_{jk}^{(i)}) = \int_{-h_i/2}^{h_i/2} (1, z_i, z_i^2) \bar{Q}_{jk} dz_i$  are the rigidity constants in which the indices  $j$  and  $k$  can be 1, 2, or 6;  $z_i$  is the transverse coordinate in the local coordinate system of the skin layers positioned at their associated mid-planes; and one should note that  $B_{jk}^{(i)} = 0$  when the planes are symmetrically laminated with respect to their mid-plane. Besides,  $\bar{Q}_{11}^{(i)} = \bar{Q}_{22}^{(i)} = \frac{E_i}{1-\nu_i^2}$ ,  $\bar{Q}_{12}^{(i)} = \frac{\nu_i E_i}{1-\nu_i^2}$ , and  $\bar{Q}_{66}^{(i)} = \frac{E_i}{2(1+\nu_i)}$ , where  $E_i$  and  $\nu_i$  are the Young modulus and Poisson ratio of the base and constraining layer, respectively. The equations of motion (2) can conveniently be written in a matrix form

$$\mathbf{Z}_{mn} \boldsymbol{\xi}_{mn} = \mathbf{q}_{mn}; \quad (3)$$

where  $\boldsymbol{\xi}_{mn} = [U_{mn}^{(1)} \ U_{mn}^{(3)} \ V_{mn}^{(1)} \ V_{mn}^{(3)} \ W_{mn}]^T$ ,  $\mathbf{q}_{mn} = [0 \ 0 \ 0 \ 0 \ q_{mn}]^T$ , and the elements of the  $(5 \times 5)$  coefficient matrix  $\mathbf{Z}_{mn} = \mathbf{a}_{mn} + \omega^2 \mathbf{b}_{mn}$  are given in the Appendix.

## 2.2. The Acoustic Radiation Problem

Let the simply-supported sandwich ERF plate be set in an infinite rigid baffle, and subjected to a harmonic point force excitation at point  $(x_0, y_0)$  with frequency  $\omega$ , i.e.  $q_0(x, y) = F_0 \delta(x - x_0) \delta(y - y_0)$ , where the associated Fourier coefficients are simply obtained as  $q_{mn} = \frac{4}{ab} \int_0^b \int_0^a q_0(x, y) \sin(\alpha_m x) \sin(\beta_n y) dx dy = \frac{4F_0}{ab} \sin(\alpha_m x_0) \sin(\beta_n y_0)$  (see Fig. 1(a)). Also, the total

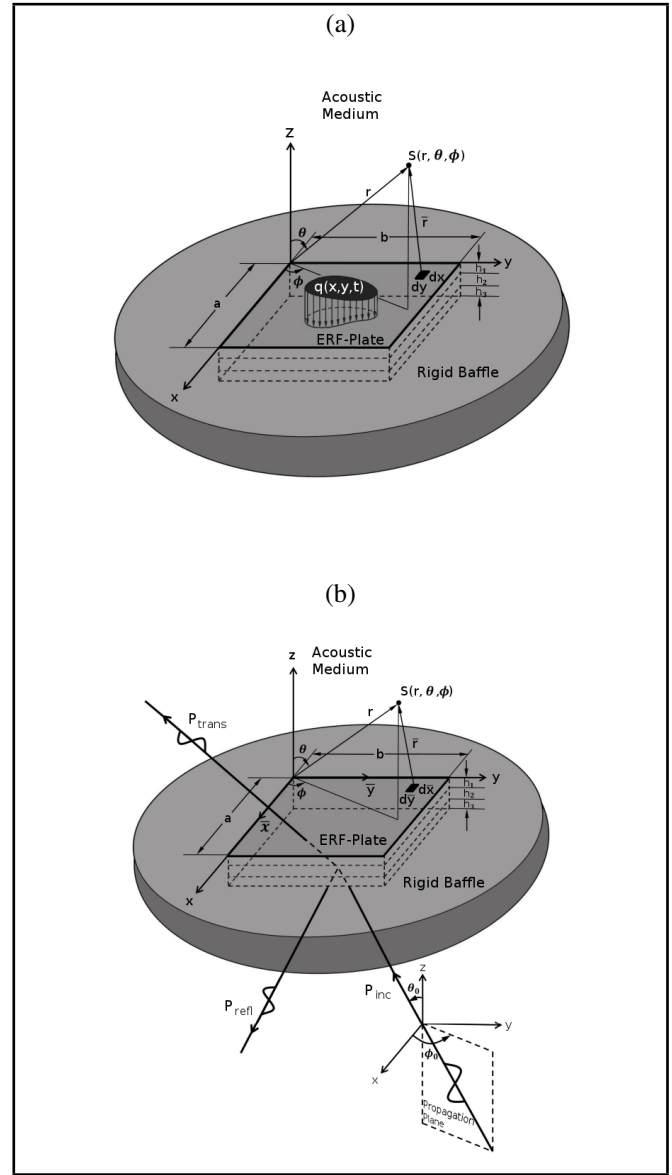


**Figure 1.** Problem geometry. (a) The acoustic radiation problem. (b) The sound transmission problem.

acoustic power radiated from the adaptive plate can be determined by integrating the far-field sound intensity over a hemisphere of radius  $r$  to get<sup>1</sup>

$$\Pi = \int_0^{2\pi} \int_0^{\pi/2} \frac{|P(r, \theta, \phi, t)|^2}{2\rho c} r^2 \sin \theta d\theta d\phi; \quad (4)$$

where  $c$  is the speed of sound in the external acoustic fluid, and  $P$  is the complex acoustic pressure at location "S" in space, expressed in spherical coordinates  $(r, \theta, \pi)$ , which can be written in terms of the plate surface velocity through the well-known Rayleigh integral in the form<sup>40</sup>

$$P(r, \theta, \phi, t) = \iint_0^a \iint_0^b \frac{i\rho k c}{2\pi \bar{r}} \frac{\partial w(x, y, t)}{\partial t} e^{-ik \bar{r}} dy dx; \quad (5)$$

where  $k = \omega/c$  is the acoustic wave number,  $\bar{r}$  is the vector connecting a representative element of the plate  $(dx, dy)$  to the field point "S" (see Fig. 1a), and using Eq. (3) with  $q_{mn} = \frac{4F_0}{ab} \sin(\alpha_m x_0) \sin(\beta_n y_0)$ , the transverse plate velocity may be

$$\begin{aligned}
 & \left(-\alpha_m^2 A_{11}^{(i)} - \beta_n^2 A_{66}^{(i)} + \rho_i h_i \omega^2\right) U_{mn}^{(i)} + \delta_i \left(-\frac{G^{(2)}}{h_2} + \frac{I_2 \omega^2}{h_2^2}\right) \left(U_{mn}^{(1)} - U_{mn}^{(3)}\right) - \alpha_m \beta_n \left(A_{12}^{(i)} + A_{66}^{(i)}\right) V_{mn}^{(i)} \\
 & + \left[\alpha_m^3 B_{11}^{(i)} + \alpha_m \delta_i \left(\frac{I_2 d \omega^2}{h_2^2} - \frac{G^{(2)} d}{h_2}\right) + \alpha_m \beta_n^2 \left(B_{12}^{(i)} + 2B_{66}^{(i)}\right)\right] W_{mn} = 0; \\
 & \left(-\alpha_m^2 A_{66}^{(i)} - \beta_n^2 A_{22}^{(i)} + \rho_i h_i \omega^2\right) V_{mn}^{(i)} + \delta_i \left(-\frac{G^{(2)}}{h_2} + \frac{I_2 \omega^2}{h_2^2}\right) \left(V_{mn}^{(1)} - V_{mn}^{(3)}\right) - \alpha_m \beta_n \left(A_{12}^{(i)} + A_{66}^{(i)}\right) U_{mn}^{(i)} \\
 & + \left[\beta_n^3 B_{22}^{(i)} + \delta_i \beta_n \left(\frac{I_2 d \omega^2}{h_2^2} - \frac{G^{(2)} d}{h_2}\right) + \alpha_m^2 \beta_n \left(B_{12}^{(i)} + 2B_{66}^{(i)}\right)\right] W_{mn} = 0; \\
 & \sum_{i=1,3} \left[\alpha_m^3 B_{11}^{(i)} + \alpha_m \beta_n^2 \left(B_{12}^{(i)} + 2B_{66}^{(i)}\right) + \delta_i \alpha_m \left(-\frac{G^{(2)} d}{h_2} + \frac{I_2 d \omega^2}{h_2^2}\right)\right] U_{mn}^{(i)} \\
 & + \sum_{i=1,3} \left[\alpha_m^2 \beta_n \left(B_{12}^{(i)} + 2B_{66}^{(i)}\right) + \beta_n^3 B_{22}^{(i)} + \delta_i \beta_n \left(-\frac{G^{(2)} d}{h_2} + \frac{I_2 d \omega^2}{h_2^2}\right)\right] V_{mn}^{(i)} \\
 & + \left\{ \sum_{i=1,3} \left[-\alpha_m^4 D_{11}^{(i)} - 2\alpha_m^2 \beta_n^2 \left(D_{12}^{(i)} + 2D_{66}^{(i)}\right) - \beta_n^4 D_{22}^{(i)}\right] - \left(\alpha_m^2 + \beta_n^2\right) \left(\frac{G^{(2)} d^2}{h_2} - \frac{I_2 d^2 \omega^2}{h_2^2}\right) \right. \\
 & \left. + \left(\rho_1 h_1 + \rho_2 h_2 + \rho_3 h_3\right) \omega^2 \right\} W_{mn} = q_{mn}; \quad (2)
 \end{aligned}$$

written in the form

$$\frac{\partial w(x, y, t)}{\partial t} = \sum_{m=1}^{\infty} \sum_{n=1}^{\infty} u_{mn} \sin(\alpha_m x) \sin(\beta_n y) e^{i\omega t}; \quad (6)$$

in which  $u_{mn} = \left(\frac{4i\omega F_0}{ab}\right) \psi(\omega) \sin(\alpha_m x_0) \sin(\beta_n y_0)$ , where  $\psi(\omega)$  is a complex (unknown) function of frequency that should be obtained by a numerical solution of the linear system of Eq. (3). Directly substituting Eq. (6) into (5), after some tedious manipulations, one obtains the final expression for the far-field acoustic pressure in the external fluid medium:<sup>3</sup>

$$P(r, \theta, \phi, t) = \sum_{m=1}^{\infty} \sum_{n=1}^{\infty} u_{mn} T_{mn}(r, \theta, \phi) e^{i\omega t}; \quad (7)$$

where

$$T_{mn}(r, \theta, \phi) = \frac{i\rho k abc}{2\pi^3 mn} \left(\frac{e^{-ikr}}{r}\right) \left[\frac{(-1)^m e^{i\mu} - 1}{\left(\frac{\mu}{n\pi}\right)^2 - 1}\right] \left[\frac{(-1)^n e^{i\chi} - 1}{\left(\frac{\chi}{m\pi}\right)^2 - 1}\right]; \quad (8)$$

in which  $\mu = ka \cdot \sin\theta \cdot \cos\phi$ , and  $\chi = kb \cdot \sin\theta \cdot \sin\phi$ . Next, direct substitution of Eq. (7) into Eq. (4), leads to the expression for total radiated power from the adaptive plate due to the action of a harmonic point force at point  $(x_0, y_0)$  in the form Eq. (9) (see the top of the next page). Now, by considering the average of all possible locations of the uncorrelated point loads acting on the plate, the total averaged radiated power is defined as<sup>14</sup>

$$\bar{\Pi} = \frac{1}{ab} \int_0^a \int_0^b \Pi(x_0, y_0) dy_0 dx_0 = \sum_{m=1}^{\infty} \sum_{n=1}^{\infty} \bar{\Pi}_{mn}; \quad (10)$$

where the modal components of the total averaged radiated power can be found by direct substitution of Eq. (9) into Eq. (10), after some manipulations, in the form<sup>14</sup>

$$\bar{\Pi}_{mn} = |u_{mn}|^2 \int_0^{2\pi} \int_0^{\pi/2} \frac{T_{mn}(r, \theta, \phi) T_{mn}^*(r, \theta, \phi)}{2\rho c} r^2 \sin\theta d\theta d\phi; \quad (11)$$

in which the cross-modal terms have been eradicated by using the classical orthogonality of transcendental eigenfunctions, and  $|u_{mn}|^2$ , which is the modulus squared of the modal velocity amplitude averaged over all force positions, is derived in the form  $\overline{|u_{mn}|^2} = \frac{1}{ab} \int_0^a \int_0^b u_{mn} u_{mn}^* dy_0 dx_0 = \left(\frac{2F_0\omega}{ab}\right)^2 \Psi_{mn}(\omega) \Psi_{mn}^*(\omega)$ . Next, using Eq. (11), the modal radiation efficiency can be written as<sup>14</sup>

$$\sigma_{mn} = \frac{\bar{\Pi}_{mn}}{\frac{1}{2}\rho cab \overline{\langle v_{mn}^2 \rangle}} = \frac{4 \int_0^{2\pi} \int_0^{\pi/2} \frac{T_{mn}(r, \theta, \phi) T_{mn}^*(r, \theta, \phi)}{(\rho c)^2 ab} r^2 \sin\theta d\theta d\phi; \quad (12)$$

where  $\overline{\langle v_{mn}^2 \rangle}$  represents the spatially-averaged modal mean square velocity, averaged over all possible force positions, obtained in the form

$$\overline{\langle v_{mn}^2 \rangle} = \frac{1}{ab} \int_0^a \int_0^b |u_{mn}|^2 \sin^2(\alpha_m x) \sin^2(\beta_n y) dy dx = \left(\frac{F_0\omega}{ab}\right)^2 \Psi_{mn}(\omega) \Psi_{mn}^*(\omega). \quad (13)$$

Direct substitution of Eq. (8) into right-hand side of Eq. (12), after some manipulations, leads to the final expression for the modal radiation efficiency in Eq. (14) (see the top of the next page). Thus, by using Eq. (12), the total average radiation efficiency of the plate is obtained in the final form

$$\sigma = \frac{\bar{\Pi}}{\frac{1}{2}\rho cab \overline{\langle v^2 \rangle}} = \frac{\sum_{m=1}^{\infty} \sum_{n=1}^{\infty} \bar{\Pi}_{mn}}{\frac{1}{2}\rho cab \overline{\langle v^2 \rangle}} = \frac{\sum_{m=1}^{\infty} \sum_{n=1}^{\infty} \sigma_{mn} \overline{\langle v_{mn}^2 \rangle}}{\overline{\langle v^2 \rangle}}; \quad (15)$$

where  $\overline{\langle v^2 \rangle} = \sum_{m=1}^{\infty} \sum_{n=1}^{\infty} \overline{\langle v_{mn}^2 \rangle}$  is the spatially-averaged mean square velocity of the plate. Here, it is noteworthy that because

$$\Pi(x_0, y_0) = \sum_{m=1}^{\infty} \sum_{n=1}^{\infty} \sum_{\bar{m}=1}^{\infty} \sum_{\bar{n}=1}^{\infty} u_{mn} u_{\bar{m}\bar{n}}^* \int_0^{2\pi} \int_0^{\pi/2} \frac{T_{mn}(r, \theta, \phi) T_{\bar{m}\bar{n}}^*(r, \theta, \phi)}{2\rho c} r^2 \sin\theta d\theta d\phi; \quad (9)$$

$$\sigma_{mn} = \frac{64k^2 ab}{\pi^6 m^2 n^2} \int_0^{\pi/2} \int_0^{\pi/2} \left\{ \frac{\sin\left(\frac{\mu}{2} + \frac{m\pi}{2}\right) \sin\left(\frac{\chi}{2} + \frac{n\pi}{2}\right)}{\left[\left(\frac{\mu}{m\pi}\right)^2 - 1\right] \left[\left(\frac{\chi}{n\pi}\right)^2 - 1\right]} \right\}^2 \sin\theta d\theta d\phi. \quad (14)$$

of the averaging over all possible force locations (see Eq. (10)), the average radiation efficiency depends only on the self-modal radiation.

### 2.3. The Sound Transmission Problem

In this subsection, the transmission loss through the simply-supported rectangular sandwich ERF plate, subjected to an obliquely incident harmonic plane wave,  $P_{inc}$ , of amplitude  $p_0$ , and the incidence angle  $(\theta_0, \phi_0)$ , as depicted in Fig. 1(b), is investigated. Also,  $P_{refl}$  and  $P_{trans}$  denote the reflected and transmitted pressure waves, respectively. These three pressure waves may be rewritten as the combination of the so-named blocked pressure (*i.e.*, the pressure on the incident side when the plate is regarded as a rigid wall) and the reradiated pressure (*i.e.*, the pressure exclusively due to the plate vibration). Making the standard assumption that the reradiated pressure is negligible compared to the blocked pressure in the equation of motion for the plate,<sup>5</sup> one can arrive at accurate solutions over a large frequency range, excluding the frequencies near the plate fundamental resonant frequency.

Adopting the three dimensional Cartesian coordinate system  $(x, y, z)$  (or equivalently the spherical coordinate system  $(r, \theta, \phi)$ ) attached to the top surface of the plate for a point S in the far-field (see Fig. 1(b)), along with the two dimensional auxiliary coordinate system  $(\bar{x}, \bar{y})$  referring to a point on the ERF plate, one can consider the equations of motion of the ERF plate (Eq. (2)) with the blocked pressure as the only forcing function in the form  $q(\bar{x}, \bar{y}, t) = P_{inc}(\bar{x}, \bar{y}, t) + P_{refl}(\bar{x}, \bar{y}, t) - P_{trans}(\bar{x}, \bar{y}, t) \approx P_b(\bar{x}, \bar{y}, t)$ , in which the blocked pressure  $P_b$  is generally assumed to be twice the incident pressure (*i.e.*,  $P_b(\bar{x}, \bar{y}, t) = 2P_{inc}(\bar{x}, \bar{y}, t)$ ).<sup>5</sup> Also, the incident travelling plane wave may be represented as in Eq. (16) (see the top of the next page),<sup>41</sup> where, with no loss of generality, the amplitude  $p_0$  of the incident pressure is taken to be a real constant. Furthermore, the generalized modal amplitude of the transverse load due to the external forcing pressure may simply be obtained from  $q(\bar{x}, \bar{y}, t) = 2P_{inc}(\bar{x}, \bar{y}, t) = \sum_{m=1}^{\infty} \sum_{n=1}^{\infty} q_{mn} \sin(\alpha_m \bar{x}) \sin(\beta_n \bar{y}) e^{i\omega t}$ , where  $q_{mn} = 8p_0 \bar{I}_m \bar{I}_n$ , in which  $\bar{I} = \frac{m\pi[1 - (-1)^m e^{-ika \sin \theta_0 \cos \phi_0}]}{(m\pi)^2 - [ka \sin \theta_0 \cos \phi_0]^2}$ ,  $\bar{I}_n = \frac{n\pi[1 - (-1)^n e^{-ikb \sin \theta_0 \sin \phi_0}]}{(n\pi)^2 - [kb \sin \theta_0 \sin \phi_0]^2}$ . The vibration of the plate causes the reradiated pressure to be transmitted by the plate. The Rayleigh integral is known to relate plate velocity to the

transmitted pressure, *i.e.*,<sup>40</sup>

$$P_{trans}(r, \theta, \phi, t) = \int_0^a \int_0^b \frac{i\rho k c}{2\pi \bar{r}} \frac{\partial w(\bar{x}, \bar{y}, t)}{\partial t} e^{-ik\bar{r}} d\bar{y} d\bar{x}. \quad (17)$$

Here, noting that  $r^2 = x^2 + y^2 + z^2$ ,  $x = r \cdot \sin\theta \cos\phi$  and  $y = r \cdot \sin\theta \sin\phi$ , one can arrive at the useful expression

$$\bar{r} = r \sqrt{1 - 2 \frac{\sin\theta \cos\phi}{r} \bar{x} - 2 \frac{\sin\theta \sin\phi}{r} \bar{y} + \left(\frac{\bar{x}}{r}\right)^2 + \left(\frac{\bar{y}}{r}\right)^2} \quad (\text{see Fig. 1(b)}).$$

As a result, a closed form evaluation of the integral shown in Eq. (17) can be obtained in the far-field by using the approximations  $1/\bar{r} \approx 1/r$ ,  $(\bar{x}/r)^2 \rightarrow 0$  and  $(\bar{y}/r)^2 \rightarrow 0$ , leading to the following expression for the far-field transmitted pressure in (18) (see the top of the next page), where the transverse plate velocity may be expanded in the form

$$\frac{\partial w(\bar{x}, \bar{y}, t)}{\partial t} = i\omega \sum_{m=1}^{\infty} \sum_{n=1}^{\infty} W_{mn} \sin(\alpha_m \bar{x}) \sin(\beta_n \bar{y}) e^{i\omega t}. \quad (19)$$

Direct substitution of the expansion in Eq. (19) into the integral representation in Eq. (18), after some manipulations, leads to

$$P_{trans}(r, \theta, \phi, t) = \frac{-\omega^2 \rho ab}{2\pi r} \exp\left[i\omega\left(t - \frac{r}{c}\right)\right] \sum_{m=1}^{\infty} \sum_{n=1}^{\infty} W_{mn} I_m I_n; \quad (20)$$

where  $I_m = \frac{m\pi[1 - (-1)^m e^{-ika \sin \theta \cos \phi}]}{(m\pi)^2 - [ka \sin \theta \cos \phi]^2}$ ,  $I_n = \frac{n\pi[1 - (-1)^n e^{-ikb \sin \theta \sin \phi}]}{(n\pi)^2 - [kb \sin \theta \sin \phi]^2}$ . Now, the total transmitted acoustic power,  $\Pi_{trans}$ , can be calculated by integrating the far-field transmitted intensity over a large hemisphere in the form<sup>1</sup>

$$\Pi_{trans} = \int_0^{2\pi} \int_0^{\pi/2} I_{trans} r^2 \sin\theta d\theta d\phi; \quad (21)$$

where the far-field transmitted intensity,  $I_{trans}$ , is given as the product of the far-field transmitted acoustic pressure and the complex conjugate of the far-field radial fluid particle velocity,  $u_r = \frac{P_{trans}}{\rho c}$ <sup>5</sup> which, by using the expansion shown in Eq. (20), reduces into

$$I_{trans} = \frac{1}{2} \text{Re} [P_{trans} u_r^*] = \frac{|P_{trans}(r, \theta, \phi, t)|^2}{2\rho c} = \frac{\rho\omega^4 a^2 b^2}{8\pi^2 r^2 c} \left| \sum_{m=1}^{\infty} \sum_{n=1}^{\infty} W_{mn} I_m I_n \right|^2. \quad (22)$$

$$P_{inc}(\bar{x}, \bar{y}, t) = p_0 \exp \left[ i \left( \omega t - k \bar{x} \sin \theta_0 \cos \phi_0 - k \bar{y} \sin \theta_0 \sin \phi_0 \right) \right]; \quad (16)$$

$$P_{trans}(r, \theta, \phi, t) = \frac{i\rho\omega}{2\pi r} \int_0^a \int_0^b \frac{\partial w(\bar{x}, \bar{y}, t)}{\partial t} \exp \left[ -ikr \left( 1 - \frac{\sin \theta \cos \phi}{r} \bar{x} - \frac{\sin \theta \sin \phi}{r} \bar{y} \right) \right] d\bar{y} d\bar{x}; \quad (18)$$

Thus, the final expression for the total transmitted acoustic power can be found by simple substitution of Eq. (22) into Eq. (21) as

$$\Pi_{trans} = \int_0^{2\pi} \int_0^{\pi/2} \frac{\rho\omega^4 a^2 b^2}{8\pi^2 c} \left| \sum_{m=1}^{\infty} \sum_{n=1}^{\infty} W_{mn} I_m I_n \right|^2 \sin \theta d\theta d\phi; \quad (23)$$

Where, for a given  $q_{mn} = 8\rho_0 \bar{I}_m \bar{I}_n$ , the unknown displacement coefficients  $W_{mn}$  can readily be obtained from the linear system of Eq. (3). Finally, the acoustic transmission loss (TL) for the baffled ERF plate can be determined from

$$TL = 10 \log \left( \frac{1}{\tau} \right); \quad (24)$$

where  $\tau = \Pi_{trans}/\Pi_{inc}$  is the transmission coefficient, and since the incident disturbance is a plane wave, the incident acoustic power,  $\Pi_{inc}$ , can simply be determined from the incident intensity multiplied by the area of the plate in the form<sup>41</sup>

$$\Pi_{inc} = \left( \frac{ab}{2\rho c} \right) p_0^2 \cos \theta_0. \quad (25)$$

In the case of a diffuse sound field, Kang, *et al.*<sup>42</sup> introduced a directional weighting function for the incident energy, leading to accurate calculation of the plate transmission loss from  $TL = 10 \log \left( \frac{1}{\tau_d} \right)$ , where the angle-averaged diffuse-field transmission coefficient,  $\tau_d(\omega)$ , which takes into account the angular characteristic of incident energy, is defined as<sup>43</sup>

$$\tau_d(\omega) = \frac{\int_0^{2\pi} \int_0^{\pi/2} D(\theta, \phi) \tau(\theta, \phi, \omega) \sin \theta \cos \theta d\theta d\phi}{\int_0^{2\pi} \int_0^{\pi/2} D(\theta, \phi) \sin \theta \cos \theta d\theta d\phi}; \quad (26)$$

in which  $D(\theta, \phi)$  signifies the directional distribution of incident sound energy, which is generally taken to be of Gaussian form with zero mean and vertical symmetry of the incident energy, *i.e.*,  $D(\theta, \phi) = e^{-\beta\theta^2}$ , where  $1 \leq \beta \leq 2$  is a constant depending on measurement parameters such as frequency, facilities dimensions, geometry, source and microphone positions.<sup>44</sup> Here, it should be noted that, in many physical situations, the diffuse sound field can be a very practical approximation to the real sound field.<sup>13,42-44</sup>

### 3. NUMERICAL RESULTS

In order to illustrate the nature and general behaviour of the solution, we consider some numerical examples in this section. Noting the large quantity of parameters and the relatively intense computations involved here, while realizing the drawbacks in accessibility of experimental input data, our attention will be focused on a specific model. A square sandwich aluminium/ERF/aluminium panel of fixed length ( $a = b = 0.5$  m)

with equal skin layer thicknesses ( $h_1 = h_3 = 0.0005$  m) set in an infinite rigid baffle is considered, while, the thickness of the ER layer is assumed to be twice that of each skin layer ( $h_2 = 0.001$  m). The material parameters for the aluminium layers are selected as  $\rho_1 = \rho_3 = 2700$  kgm<sup>3</sup>;  $E_1 = E_3 = 70$  GPa;  $\nu_1 = \nu_3 = 0.3$ . Also, using the accessible information on the ER material pre-yield rheology, the electric field dependence of ER material in the pre-yield regime is considered. In particular, the complex modulus for a typical ER fluid is adopted from Yalcintas and Coulter's work<sup>45</sup> in the form

$$G^{(2)}(E) = G'(E) + iG''(E); \quad (27)$$

where  $G'(E) = 50,000 E^2$  is the shear storage modulus,  $G''(E) = 2600 E + 1700$  is the loss modulus, and  $0 \leq E(t) \leq 3.5$  kV/mm is the electric field strength. Also,  $\rho_2 = 1700$  kg/m<sup>3</sup> is the mass density of the ER fluid. In addition, the surrounding fluid medium is assumed to be air at atmospheric pressure and ambient temperature ( $\rho = 1.2$  kg/m<sup>3</sup>,  $c = 340$  m/s).

A Mathematica code was constructed for treating the linear system of Eq. (3), solving for the unknown transverse modal displacement coefficients  $W_{mn}$  as functions of the incident wave angles and frequency (or external loading frequency in the radiation problem) as well as the electric field magnitude, and ultimately calculating the spatially-averaged mean square velocity of the plate,  $\langle \bar{v}^2 \rangle$ , the total average radiation efficiency,  $\sigma$ , and the acoustic transmission loss, TL, for the above selected geometric parameters. Also, the value of the exponential parameter,  $\beta = 2$ , is selected for a perfectly diffuse sound field,<sup>44</sup> and the integrals in Eqs. (23) and (26) were numerically evaluated using the Mathematica built-in function "NIntegrate." The convergence of results was systematically checked in a simple trial-and-error manner, by increasing the truncation constants in the Fourier expansions, while looking for steadiness or stability in the numerical value of the solutions. Using a maximum number of thirty modes, ( $m_{max} = n_{max} = 30$ ) was found to yield satisfactory results for the selected geometric parameters in all loading situations.

Before presenting the main numerical results, we shall briefly check the overall validity of the work. To do this, we first used our general "sound transmission" Mathematica code to compute the sound transmission loss for a three-layered aluminium-ERF-aluminium plate (with its physical properties as given in Table 1), under a selected electric field strength ( $E = 0.5$  kV/mm) and incidence angles ( $\theta_0 = \phi_0 = 60^\circ$ ), as shown in the first subplot of Fig. 2(a). Furthermore, we used our general "sound radiation" Mathematica code to compute the mean square velocity,  $\langle \bar{v}^2 \rangle$ , for the three-layered adaptive plate, under a selected electric field strength ( $E = 0.5$  kV/mm) and for a unit amplitude harmonic load ( $F_0 = 1$ ), as shown in the second subplot of Fig. 2(a). It is clear that the ERF plate resonance frequencies show up as dips in the Transmis-

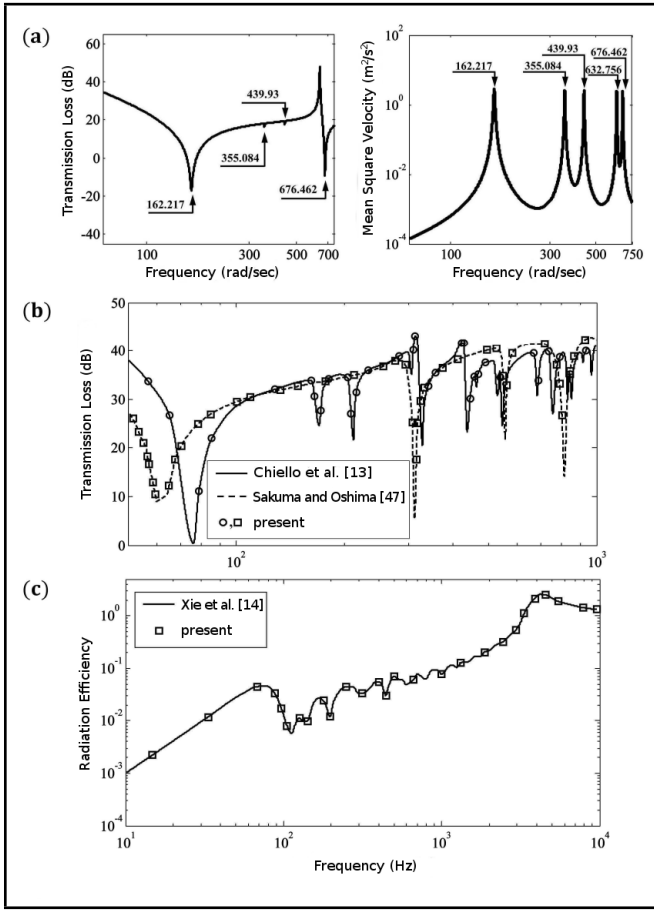


**Figure 2.** (a) Sound transmission loss and mean square velocity spectrum for a three-layered aluminium-ERF-aluminium plate under selected electric field strength ( $E = 0.5$  kV/mm) and incidence angles ( $\theta_0 = \phi_0 = 60^\circ$ ;  $F_0 = 1$ ). (b) Comparison of the calculated sound transmission loss of a single-layer panel with those available in the literature. (c) Comparison of the calculated radiation efficiency of a single-layer panel with that available in the literature.

sion Loss (TL) subplot and peaks in the mean square velocity subplot, as marked in the figures, and demonstrate very good agreements with the natural frequencies displayed in Fig. 5 of the work of Yeh and Chen,<sup>46</sup> which were obtained by means of the finite element method. As a further verification, we let the bottom and midlayer thickness values of the adaptive plate approach zero ( $h_2 = h_3 \approx 0$ ) in our general "sound transmission" code, and calculated the Transmission Loss (TL) spectra for normal incidence as well as for the diffuse case ( $D(\theta, \phi) = 1$ ) for single-layered aluminium plates with their physical properties, as shown in Table 2. The outcome, as displayed in Fig. 2(b), shows very good agreement with the Transmission Loss (TL) data presented in Figs. 3 and 6 in the works of Chiello, Sgard, and Atalla<sup>13</sup> and Sakuma and Oshima,<sup>47</sup> respectively. Lastly, we let the bottom and mid-layer thickness values approach zero in our general "sound radiation" code, and calculated the average radiation efficiency,  $\sigma$ , for a single-layered aluminium plate with its physical properties as given in Table 3. The outcome, as shown in Fig. 2(c) shows excellent agreement with the data presented in Fig. 3 of the study conducted by Xie, Thompson, and Jones.<sup>14</sup>

Figure 3 shows the variation of sound transmission loss (TL) with incident wave frequency for selected angles of incidence ( $\theta_0 = 0, 45, 80$ ;  $\phi_0 = 0, 45^\circ$ ), and for applied electric field strengths ( $E = 0, 1, 2, 3.5$  kV/mm). Also shown are the TL spectra calculated for the ERF panel in a perfectly diffuse

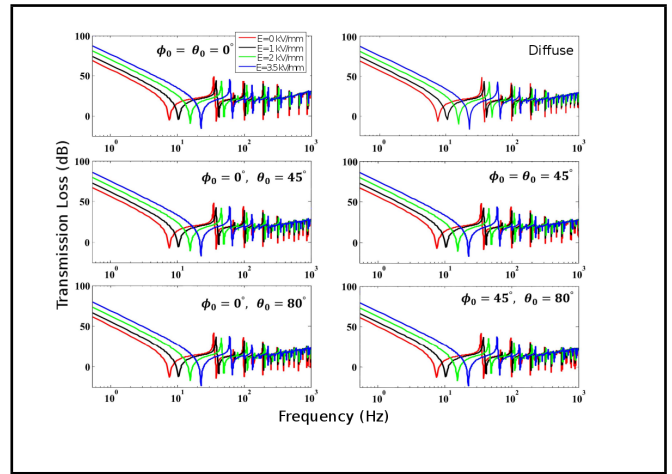


**Figure 3.** Variation of sound transmission loss with incident wave frequency for selected angles of incidence (including the perfectly diffuse situation) and applied electric field strengths.

**Table 1.** Input physical properties used for the verification example presented in Fig. 2(a).

$a = 0.3$ m
$b = 0.25$ m
$h_1 = 0.00005$ m
$h_2 = h_3 = 0.0005$ m
$E_1 = E_3 = 70$ GPa
$\nu_1 = \nu_3 = 0.3$
$\rho_1 = \rho_3 = 2700$ kg/m <sup>3</sup>
$\rho = 1.2$ kg/m <sup>3</sup>
$c = 340$ m/s
$\theta_0 = \phi_0 = 60^\circ$
$E = 0.5$ kV/mm

**Table 2.** Input physical properties used for the verification examples presented in Fig. 2(b).

Chiello, Sgard, and Atalla <sup>13</sup>
$a = 0.48$ m
$b = 0.4$ m
$h_1 = 0.003$ m
$h_2 = h_3 = 3 \times 10^{-7}$ m
$E_1 = E_3 = 200(1+0.01i)$ GPa
$\nu_1 = \nu_3 = 0.3$
$\rho_1 = \rho_3 = 7800$ kg/m <sup>3</sup>
$\rho = 1.2$ kg/m <sup>3</sup>
$c = 340$ m/s
$E = 0$ kV/mm
Sakuma and Oshima <sup>47</sup>
$a = b = 0.9$ m
$h_1 = 0.01$ m
$h_2 = h_3 = 10^{-6}$ m
$E_1 = E_3 = 75(1+0.002i)$ GPa
$\nu_1 = \nu_3 = 0.22$
$\rho_1 = \rho_3 = 2500$ kg/m <sup>3</sup>
$\rho = 1.2$ kg/m <sup>3</sup>
$c = 340$ m/s
$\theta_0 = \phi_0 = 0^\circ$
$E = 0$ kV/mm

**Table 3.** Input physical properties used for the verification example presented in Fig. 2(c).

$a = 0.5$ m
$b = 0.6$ m
$h_1 = 0.003$ m
$h_2 = h_3 = 3 \times 10^{-7}$ m
$E_1 = E_3 = 71(1+0.1i)$ GPa
$\nu_1 = \nu_3 = 0.3$
$\rho_1 = \rho_3 = 2700$ kg/m <sup>3</sup>
$\rho = 1.2$ kg/m <sup>3</sup>
$c = 340$ m/s
$E = 0$ kV/mm

sound field. The most important observations are as follows: The application of the electric field appears to have an appreciable effect on sound transmission, especially in the very low frequency range ( $f < 30$  Hz). In particular, increasing the electric field strength at such low frequencies leads to a distinct monotonic increase in the TL amplitudes, nearly regardless of the angle of incidence. This may clearly be linked to the increase in the overall structural stiffness of the system in the so-named stiffness controlled region.<sup>1</sup> As the incident wave frequency increases, the effect of the electric field gradually decreases, especially for the case of normal incidence, where there is minimum shear effect induced in the ERF core layer. In the very high frequency range ( $f > 1000$  Hz), increasing the electric field has a small effect on the TL amplitudes for all angles of incidence. This is perhaps due to the fact that at such high frequencies, the plate inertia effects overwhelms the electric field effects.

Also, it is well known that the incidence angle has a notable effect on the excitation of panel vibrational modes. In the case of normal incidence, the sound pressure imposed on the panel is uniform, and thus only the odd-odd panel modes are expected to be excited (to transmit sound power). Furthermore, in the case of oblique incidence with the incident wave traveling parallel to the  $x$ -axis (*i.e.*, for  $\phi_0 = 0^\circ$ ), the radiated power for even-even or odd-even modes of the panel is rather small, and the resonance dips in the calculated TL take place at the resonance frequencies whose  $y$ -axis mode numbers are odd. Likewise, the resonance dips in the calculated TL for incident waves travelling parallel to the  $y$ -axis (*i.e.*, for  $\phi_0 = 90^\circ$ ) happen at the resonance frequencies whose  $x$ -axis mode numbers are odd. Keeping the above discussion in mind, one can readily see from Fig. 3 that for non-normal incident wave fields, many more plate resonance frequencies get involved (note the numerous dips appearing in the sub-figures), as either the inclination angle,  $\theta_0$ , or the azimuth angle,  $\phi_0$ , increases, nearly regardless of the electric field strength. Moreover, the smallest TL levels are observed in case of the near-grazing ( $\theta_0 = 80^\circ$ ) incident wave field, while decreasing the inclination angle,  $\theta_0$ , has a slight amplification effect on the panel sound transmission loss, especially at low incident wave frequencies (thus, the largest overall TL levels are observed in case of the normally incident, or  $\theta_0 = 0^\circ$ , sound field). The TL curves for the perfectly diffuse or random sound field behave rather differently, recalling that a diffuse sound field superposes a series of equal-amplitude uncorrelated progressive plane waves, with all directions of sound propagation arising with the same probability, and the phase relations of the waves being arbitrary at any given point in space.<sup>42-44</sup>

In particular, in the low frequency region ( $f < 100$  Hz), the TL levels associated with the diffuse field are very close to those of the normally incident ( $\theta_0 = 0^\circ$ ) case, where mainly the uniform odd-odd panel modes seem to be excited. In the higher frequency range ( $f > 100$  Hz), on the other hand, the TL curves of the diffuse sound field behave very similarly to those of the near-grazing ( $\theta_0 = 80^\circ$ ) incident sound field, where the appearance of the numerous dips indicate that increasingly more panel resonance frequencies get involved (*i.e.*, sound transmission is mainly controlled by panel resonant effects<sup>48</sup>). This similarity in the sound transmission characteristics of the diffuse and near-grazing incidence problems can also be observed in Fig. 5 of the work of Schiller and Beck.<sup>49</sup>

Therefore, in the mid- to high-frequency range, it may be sufficient to use the near-grazing incidence TL with an acceptable error (or with a correction factor) in order to predict the diffuse field transmission loss, nearly regardless of the electric field strength.

At each incident wave frequency, there is only one electric field level which leads to a maximum or a minimum transmission loss amplitude, denoted here by  $E_{max}$  (kV/mm) or  $E_{min}$  (kV/mm), respectively. The left column in Fig. 4 displays the variations in sound transmission loss (TL) amplitude with the incident wave frequency associated with such electric field strengths, for the adaptive plate under selected angles of incidence ( $\theta_0 = 45^\circ$ ;  $\phi_0 = 0, 45^\circ$ ) as well as for the perfectly diffuse field (note that the TL associated with the  $E = 0$  kV/mm case is also shown in the figure by black lines). Moreover, the right column of Fig. 4 depicts the frequency spectrums of the corresponding input electric field amplitudes required for maximizing or minimizing sound transmission loss. The most important observations are as follows: Perfect coincidence of the black curves ( $E = 0$ ) with the blue curves ( $E = E_{min}$ ) in the entire low frequency range (*i.e.*, in the stiffness-controlled region) as well as in some relatively small frequency patches in the moderate and high frequency range leads to the important conclusion that maintaining a null electric field level (*i.e.*, keeping the panel stiffness low) can significantly deteriorate the sound transmission performance of the ERF-based plate, primarily in the low frequency range.

In other words, it is clear that inappropriate application of the electric field (*e.g.*, note the blue curves associated with  $E = E_{min}$ ) may even lead to minimum sound transmission loss levels in a wide frequency range. The most interesting observation is perhaps the fact that by selecting  $E = E_{max}$  (*i.e.*, the red colored curves), one can advantageously avoid the commonly occurring sharp (resonant) dips in the uncontrolled ( $E = 0$ ) or non-optimally controlled ( $E \neq E_{max}$ ) adaptive structure, leading to maximum transmission loss in the entire frequency range, nearly irrespective of incident wave direction. Moreover, the maximum or minimum electrical field pattern (shown in the second column of the figure) resembles a repeating ramp type curve, while the effect of incident wave direction on the electric field strength is not very prominent. Furthermore, repeated zones of a null electric field ( $E = 0$  kV/mm) are observed in the entire frequency range, which are associated with either a maximum or a minimum sound transmission loss level. Thus, one can conversely conclude that applying a non-zero electric field (*i.e.*, increasing the structural stiffness and damping), does not necessarily lead to an improvement in the system's sound transmission characteristics.

Figures 5(a) and (b) show the variation of total average radiation efficiency,  $\sigma$ , as well as the average mean square velocity,  $\langle v^2 \rangle$ , with the external load frequency ( $F_0 = 1$  N), for selected applied electric field strengths ( $E = 0, 1, 2, 3.5$  kV/mm). The most important observations are as follows: While the electric field strength has little or nearly no effect on the average radiation efficiency spectrum at low and high frequency ends (Fig. 5(a)), it is of significant influence on the average mean square velocity in the entire frequency range (Fig. 5(b)). In particular, the electric field seems to be of major consequence on the radiation efficiency only in the intermediate frequency range (*i.e.*, increasing the electric field strength has a notable

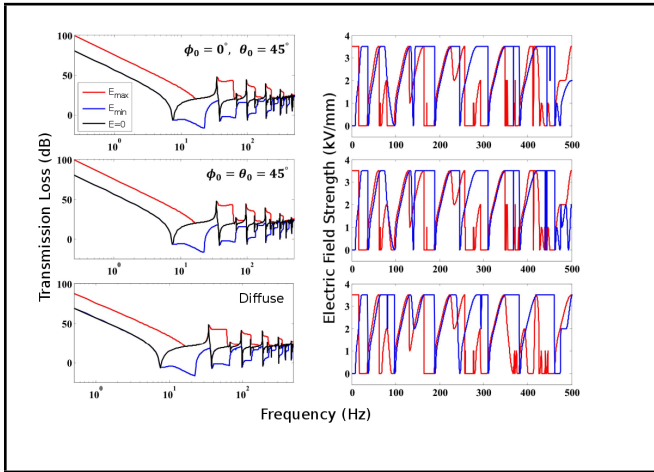


**Figure 4.** Calculated maximum and minimum sound transmission loss spectrums for selected angles of incidence (including the perfectly diffuse field) along with the associated applied electric fields.

amplification effect on the sandwich plate radiation efficiency roughly in the range of  $10 < f < 100$  Hz; see Fig. 5(a)). This may be explained by comparison with Fig. 5(b), where it is clear that increasing the electric field level (increasing or decreasing the overall system stiffness and displacement amplitudes) leads to a notable rightward shift in the resonance frequencies of an adaptive plate (*i.e.*, the peaks in the mean square velocity curves) to the higher frequency range (see Hasheminejad and Maleki<sup>38</sup>).

Moreover, there is a notable decrease in the oscillation amplitude of the mean square velocity curves with increasing the electric field strength towards  $E = 3.5$  kV/mm (or increasing overall system stiffness) at intermediate and low frequencies, which may be linked to the overall decrease in the system kinetic energy. Thus, one may conclude that while direct application of an electric field can perceptibly influence the radiation efficiency of an adaptive panel in the intermediate frequency range, it can effectively reduce the average mean square velocity in the entire frequency range. Lastly, as the excitation frequency further increases, approaching the system critical frequency ( $f_c = \omega_c 2\pi \approx 11.9$  kHz; as observed from Fig. 5(a)), the occurrence of 'edge' modes dominate the so-called corner modes,<sup>1</sup> and the electric field strength almost entirely loses its effect on the sound radiation efficiency, which gradually increases towards its maximum level slightly beyond the critical frequency and then makes a small drop towards the asymptotic value of unity.<sup>43</sup>

As in the case of the previously discussed sound transmission problem (see Fig. 4), at each excitation frequency there is only one electric field level which causes a maximum or minimum average radiation efficiency or a maximum or minimum mean square velocity, denoted here by  $E_{max}^\sigma/E_{min}^\sigma$  kV/mm or  $E_{max}^v/E_{min}^v$  kV/mm, respectively. The left column in Fig. 6 displays the variations in the total average radiation efficiency,  $\sigma$ , as well as the average mean square velocity,  $\langle v^2 \rangle$ , with the excitation frequency associated with such electric field strengths (note that the results associated with the  $E = 0$  kV/mm case are also shown in the subplots by black lines). Moreover, the right column of Fig. 6 depicts the frequency spectrums of the corresponding electric field amplitudes calculated for maximizing or minimizing the average radiation efficiency or the mean square velocity. Here, the nearly

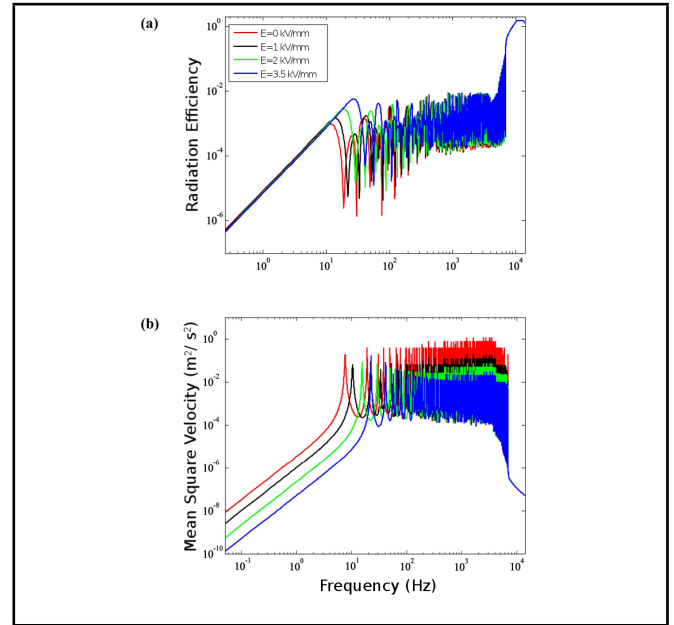


**Figure 5.** (a) Variation of the total average radiation efficiency with the external load frequency for selected applied electric field strengths. (b) Variation of the average mean square velocity with the external load frequency for selected applied electric field strengths.

perfect coincidence of the black curve ( $E = 0$ ) with the red and blue curves ( $E = E_{min,max}^\sigma$ ) in the entire low frequency range (*i.e.*, in the stiffness-controlled region) once again leads to the important conclusion that the electric field level has nearly no effect on the sound radiation performance of the ERF-based plate in the low frequency range.

Furthermore, almost perfect coincidence of the maximum mean square velocity ( $E = E_{max}^v$  or the red) curve with that of the null field ( $E = 0$  or the black curve) in the low frequency range demonstrates that decreasing the electric field strength (system stiffness) leads to a natural increase in the system mean square velocity. Also, it is clear that as in the case of the sound transmission problem (Fig. 4), inappropriate application of the electric field may deteriorate sound radiation efficiency in a wide frequency range (*i.e.*, note the blue curve associated with  $E = E_{min}^\sigma$ ). Another interesting observation is the fact that by selecting  $E = E_{max}^\sigma$  or  $E = E_{max}^v$  (*i.e.*, the red colored curves), one can respectively avoid the commonly occurring sharp dips or peaks in the uncontrolled or non-optimally controlled adaptive structure, leading to maximum radiation efficiency (or mean square velocity) in the entire frequency range.

#### 4. CONCLUSIONS

The three-dimensional sound radiation and transmission control from and through an electrorheological fluid-based rectangular sandwich plate, set in an infinite rigid baffle, and subjected to a periodic transverse excitation or an arbitrary incident plane wave, is considered in this study. The problem solution is based on the equations of motion for a simply-supported ERF-based plate, the classical complex modulus approach for the viscoelastic behaviour of ER core fluid, the pertinent wave field expansions, and the modal summation method along with the Rayleigh integral equation approach. Special attention is paid to the influence of electric field strength, incident wave angle (including the perfectly diffuse

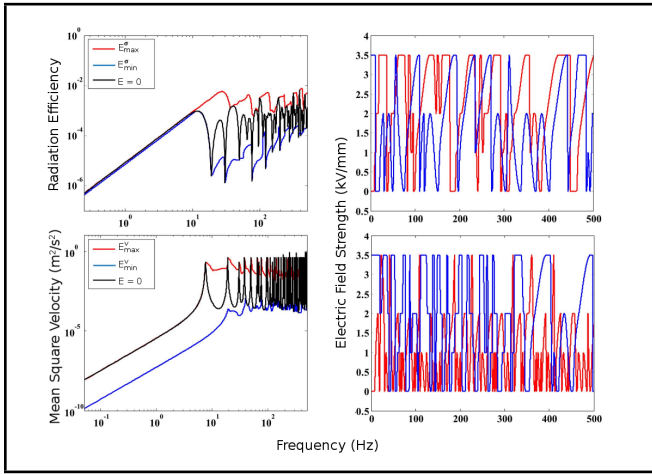


**Figure 6.** Calculated maximum and minimum average radiation efficiency and mean square velocity spectrums along with the associated applied electric fields.

situation) and excitation frequency on the sound transmission and radiation characteristics of the adaptive panel. The most important observations regarding the sound transmission and radiation problem are respectively summarized in the following two paragraphs.

Increasing the electric field strength at very low incident wave frequencies (*i.e.*, in the stiffness controlled region) leads to a distinct monotonic increase in the sound transmission amplitudes, nearly regardless of angle of incidence, caused by the increase in the overall structural stiffness of the system. As the incident wave frequency increases, the electric field effect gradually decreases, especially in cases of normal incidence, where there is minimum shear effect induced in the ERF core layer. In the very high frequency range ( $f > 1000$  Hz), the plate inertia effects dominate the electric field effects and the electric field level is observed to have a small influence on the sound transmission loss, almost regardless of the angle of incidence. In case of normal incidence, only the odd-type plate modes are observed to get excited, while for oblique incidence (non-zero inclination angle), even-type modes can also get involved, the extent of which depends on the azimuth angle. Also, as the obliquity of the incident wave increases, the sound transmission loss amplitudes generally decrease, nearly regardless of the electric field strength, especially at high incident wave frequencies. In particular, the largest TL levels are found in case of the normally incident sound field.

Furthermore, in the low frequency range, the TL levels associated with the diffuse sound field are observed to be very close to those of the normally incident case, while the panel resonant effects dominate at higher frequencies, and the TL curves of the diffuse field behave very similarly to those of the near-grazing incidence situation. Therefore, in order to approximate the diffuse field transmission loss with an acceptable error in the mid- to high-frequency range, it may be sufficient to use the near-grazing incidence TL, nearly regardless of the electric field strength. Lastly, maintaining a null electric field level is shown to significantly deteriorate the sound transmission performance of the ERF-based plate, primarily in the low frequency range, while applying a non-zero electric field does not necessarily lead to an improvement in the system's overall sound transmission characteristics.

The electric field strength has little or nearly no effect on

the average radiation efficiency spectrum at low and high frequency ends, while it can effectively reduce the average mean square panel velocity in the entire frequency range. In particular, increasing the electric field strength is demonstrated to have a notable amplification effect on the adaptive plate radiation efficiency in the intermediate frequency region ( $10 < f < 100$  Hz). It also causes a notable rightward shift in the resonance frequencies appearing in the mean square velocity plot of the adaptive plate in addition to a general drop in velocity amplitudes. As the excitation frequency approaches the system critical frequency, the occurrence of 'edge' modes dominate the so-called corner modes, and the electric field strength almost entirely loses its effect on the system sound radiation efficiency, which gradually increases towards its maximum level slightly beyond the critical frequency and then makes a small drop towards the asymptotic value of unity. Lastly, by adopting the optimal electric field strength, one can advantageously avoid the commonly occurring sharp resonant peaks and dips in the radiation spectrum of the uncontrolled or non-optimally controlled adaptive structure, resulting in major improvements in the system's overall sound radiation characteristics. It is hoped that the present study will provide designers the basic information required in practical noise control applications of ER fluid-embedded smart structures.

## APPENDIX

$$\begin{aligned}
 a_{mn}^{11} &= -\alpha_m^2 A_{11}^{(1)} - \beta_n^2 A_{66}^{(1)} - G^{(2)}/h_2, \\
 a_{mn}^{12} &= G^{(2)}/h_2, \\
 a_{mn}^{13} &= -\alpha_m \beta_n (A_{12}^{(1)} + A_{66}^{(1)}), \\
 a_{mn}^{14} &= 0, \\
 a_{mn}^{15} &= \alpha_m^3 B_{11}^{(1)} - \alpha_m G^{(2)}d/h_2 + \alpha_m \beta_n^2 (B_{12}^{(1)} + 2B_{66}^{(1)}), \\
 a_{mn}^{21} &= G^{(2)}/h_2, \\
 a_{mn}^{22} &= -\alpha_m^2 A_{11}^{(3)} - \beta_n^2 A_{66}^{(3)} - G^{(2)}/h_2, \\
 a_{mn}^{23} &= 0, \\
 a_{mn}^{24} &= -\alpha_m \beta_n (A_{12}^{(3)} + A_{66}^{(3)}), \\
 a_{mn}^{25} &= \alpha_m^3 B_{11}^{(3)} + \alpha_m G^{(2)}d/h_2 + \alpha_m \beta_n^2 (B_{12}^{(3)} + 2B_{66}^{(3)}), \\
 a_{mn}^{31} &= -\alpha_m \beta_n (A_{12}^{(1)} + A_{66}^{(1)}), \\
 a_{mn}^{32} &= 0, \\
 a_{mn}^{33} &= -\alpha_m^2 A_{66}^{(1)} - \beta_n^2 A_{22}^{(1)} - G^{(2)}/h_2, \\
 a_{mn}^{34} &= G^{(2)}/h_2, \\
 a_{mn}^{35} &= \alpha_m^2 \beta_n (B_{12}^{(1)} + 2B_{66}^{(1)}) + \beta_n^3 B_{22}^{(1)} - \beta_n G^{(2)}d/h_2, \\
 a_{mn}^{41} &= 0, \\
 a_{mn}^{42} &= -\alpha_m \beta_n (A_{12}^{(3)} + A_{66}^{(3)}), \\
 a_{mn}^{43} &= G^{(2)}/h_2, \\
 a_{mn}^{44} &= -\alpha_m^2 A_{66}^{(3)} - \beta_n^2 A_{22}^{(3)} - G^{(2)}/h_2, \\
 a_{mn}^{45} &= \alpha^2 \beta_n (B_{12}^{(3)} + 2B_{66}^{(3)}) + \beta_n^3 B_{22}^{(3)} + \beta_n G^{(2)}d/h_2, \\
 a_{mn}^{51} &= \alpha_m^3 B_{11}^{(1)} + \alpha_m \beta_n^2 (B_{12}^{(1)} + 2B_{66}^{(1)}) - \alpha_m G^{(2)}d/h_2, \\
 a_{mn}^{52} &= \alpha_m^3 B_{11}^{(3)} + \alpha_m \beta_n^2 (B_{12}^{(3)} + 2B_{66}^{(3)}) + \alpha_m G^{(2)}d/h_2, \\
 a_{mn}^{53} &= \alpha_m^2 \beta_n (B_{12}^{(1)} + 2B_{66}^{(1)}) + \beta_n^3 B_{22}^{(1)} - \beta_n G^{(2)}d/h_2, \\
 a_{mn}^{54} &= \alpha_m^2 \beta_n (B_{12}^{(3)} + 2B_{66}^{(3)}) + \beta_n^3 B_{22}^{(3)} + \beta_n G^{(2)}d/h_2,
 \end{aligned}$$

$$a_{mn}^{55} = -\alpha_m^4 \left( D_{11}^{(1)} + D_{11}^{(3)} \right) + \\ -2\alpha_m^2 \beta_n^2 \left( D_{12}^{(1)} + D_{12}^{(3)} + 2D_{66}^{(1)} + 2D_{66}^{(3)} \right) \\ -\beta_n^4 \left( D_{22}^{(1)} + D_{22}^{(3)} \right) - (\alpha_m^2 + \beta_n^2) G^{(2)} d^2 / h_2,$$

and

$$b_{mn}^{11} = \rho_1 h_1 + I_2 / h_2^2, \\ b_{mn}^{12} = -I_2 / h_2^2, \\ b_{mn}^{13} = b_{mn}^{14} = 0, \\ b_{mn}^{15} = \alpha_m I_2 d / h_2^2, \\ b_{mn}^{21} = -I_2 / h_2^2, \\ b_{mn}^{22} = \rho_3 h_3 + I_2 / h_2^2, \\ b_{mn}^{23} = b_{mn}^{24} = 0, \\ b_{mn}^{25} = -\alpha_m I_2 d / h_2^2, \\ b_{mn}^{31} = b_{mn}^{32} = 0, \\ b_{mn}^{33} = \rho_1 h_1 + I_2 / h_2^2, \\ b_{mn}^{34} = -I_2 / h_2^2, \\ b_{mn}^{35} = \beta_n I_2 d / h_2^2, \\ b_{mn}^{41} = b_{mn}^{42} = 0, \\ b_{mn}^{43} = -I_2 / h_2^2, \\ b_{mn}^{44} = \rho_3 h_3 + I_2 / h_2^2, \\ b_{mn}^{45} = -\beta_n I_2 d / h_2^2, \\ b_{mn}^{51} = \alpha_m I_2 d / h_2^2, \\ b_{mn}^{52} = -\alpha_m I_2 d / h_2^2, \\ b_{mn}^{53} = \beta_n I_2 d / h_2^2, \\ b_{mn}^{54} = -\beta_n I_2 d / h_2^2, \\ b_{mn}^{55} = (\alpha_m^2 + \beta_n^2) I_2 d^2 / h_2^2 + (\rho_1 h_1 + \rho_2 h_2 + \rho_3 h_3).$$

## REFERENCES

- 1 Fahy, F. and Gardonio, P. *Sound and structural vibration: Radiation, transmission and response*, Academic Press, Oxford, 2007, 2<sup>nd</sup> ed. <http://dx.doi.org/10.3397/1.2741307>
- 2 Maidanik, G. Response of ribbed panels to reverberant acoustic fields, *J. Acoust. Soc. Am.*, **34** (6), 809–826, (1962). <http://dx.doi.org/10.1121/1.1918200>
- 3 Wallace, C. E. Radiation resistance of rectangular panel, *J. Acoust. Soc. Am.*, **51** (3), 946–952, (1972). <http://dx.doi.org/10.1121/1.1912943>
- 4 Leppington, F. G., Broadbent, E. G., and Heron, K. H. The acoustic radiation efficiency of rectangular panels, *Proc. Roy. Soc. London, Ser. A*, **382** (1783), 245–271, (1982). <http://dx.doi.org/10.1098/rspa.1982.0100>
- 5 Roussos, L. A. Noise transmission loss of a rectangular plate in an infinite baffle, *J. Acoust. Soc. Am.*, **75** (S1), S2, (1984). <http://dx.doi.org/10.1121/1.2021367>
- 6 Panneton, R. and Atalla, N. Numerical prediction of sound transmission through finite multilayer systems with poroelastic materials, *J. Acoust. Soc. Am.*, **100** (1), 346–354, (1996). <http://dx.doi.org/10.1121/1.415956>
- 7 Lee, C. and Kondo, K. Noise transmission loss of sandwich plates with viscoelastic core, *40th Struct., Struct. D., and Mat. Conf. and Ex., Struct., Struct. D., and Mat. and Co-located Conf.*, 2137–2147, (1999). <http://dx.doi.org/10.2514/6.1999-1458>
- 8 Foin, O., Nicolas, J., and Atalla, N. An efficient tool for predicting the structural acoustic and vibration response of sandwich plates in light or heavy fluid, *Appl. Acoust.*, **57** (3), 213–242, (1999). [http://dx.doi.org/10.1016/S0003-682X\(98\)00059-0](http://dx.doi.org/10.1016/S0003-682X(98)00059-0)
- 9 Foin, O., Berry, A., and Szabo, J. Acoustic radiation from an elastic baffled rectangular plate covered by a decoupling coating and immersed in a heavy acoustic fluid, *J. Acoust. Soc. Am.*, **107** (51), 2501–2510, (2000). <http://dx.doi.org/10.1121/1.428638>
- 10 Sgard, F. C., Atalla, N., and Nicolas, J. A numerical model for the low frequency diffuse field sound transmission loss of double-wall sound barriers with elastic porous linings, *J. Acoust. Soc. Am.*, **108** (6), 2865–2872, (2000). <http://dx.doi.org/10.1121/1.1322022>
- 11 Berry, A., Foin, O., and Szabo, J. P. Three-dimensional elasticity model for a decoupling coating on a rectangular plate immersed in a heavy fluid, *J. Acoust. Soc. Am.*, **109** (6), 2704–2714, (2001). <http://dx.doi.org/10.1121/1.1372224>
- 12 Park, J., Mongeau, L., and Siegmund, T. Influence of supported properties on the sound radiated from the vibration of rectangular plates, *J. Sound Vib.*, **275** (1–2), 249–265, (2004). [http://dx.doi.org/10.1016/S0022-460X\(02\)01215-4](http://dx.doi.org/10.1016/S0022-460X(02)01215-4)
- 13 Chiello, O., Sgard, F. C., and Atalla, N. On the use of a component mode synthesis technique to investigate the effects of elastic boundary conditions on the transmission loss of baffled plates, *Comput. Struct.*, **81** (28–29), 2645–2658, (2003). [http://dx.doi.org/10.1016/S0045-7949\(03\)00326-2](http://dx.doi.org/10.1016/S0045-7949(03)00326-2)
- 14 Xie, G., Thompson, D. J., and Jones, C. J. C. The radiation efficiency of baffled plates and strips, *J. Sound Vib.*, **280** (1–2), 181–209, (2005). <http://dx.doi.org/10.1016/j.jsv.2003.12.025>
- 15 Au, F. T. K. and Wang, M. F. Sound radiation from forced vibration of rectangular orthotropic plates under moving loads, *J. Sound Vib.*, **281** (3–5), 1057–1075, (2005). <http://dx.doi.org/10.1016/j.jsv.2004.02.005>
- 16 Park, J. and Mongeau, L. Vibration and sound radiation of viscoelastically supported Mindlin plates, *J. Sound Vib.*, **318** (4–5), 1230–1249, (2008). <http://dx.doi.org/10.1016/j.jsv.2008.04.045>
- 17 Assaf, S. and Guerich, M. Numerical prediction of noise transmission loss through viscoelastically damped sandwich plates, *J. Sandw. Struct. Mater.*, **10** (5), 359–384, (2008). <http://dx.doi.org/10.1177/1099636207088444>
- 18 Chazot, J. D. and Guyader, J. L. Transmission loss of double panels filled with poroelastic materials, *J. Acoust. Soc. Am.*, **126** (6), 3040–3048, (2009). <http://dx.doi.org/10.1121/1.3245033>
- 19 Assaf, S., Guerich, M., and Cuvelier, P. Vibration and acoustic response of damped sandwich plates immersed in a light or heavy fluid, *Comput. Struct.*, **88** (13–14), 870–878, (2010). <http://dx.doi.org/10.1016/j.compstruc.2010.04.006>
- 20 Zhou, R. and Crocker, M. J. Boundary element analyses for sound transmission loss of panels, *J. Acoust. Soc. Am.*, **127** (2), 829–840, (2010). <http://dx.doi.org/10.1121/1.3273885>

- <sup>21</sup> Loredo, A., Plessy, A., Hafidi, A. E., and Hamzaoui, N. Numerical vibroacoustic analysis of plates with constrained-layer damping patches, *J. Acoust. Soc. Am.*, **129** (4), 1905–1918, (2011). <http://dx.doi.org/10.1121/1.3546096>
- <sup>22</sup> Li, S. Active modal control simulation of vibro-acoustic response of a fluid-loaded plate, *J. Sound Vib.*, **330** (23), 5545–5557, (2011). <http://dx.doi.org/10.1016/j.jsv.2011.07.001>
- <sup>23</sup> Kam, T. Y., Jiang, C. H., Lee, B. Y. Vibro-acoustic formulation of elastically restrained shear deformable stiffened rectangular, *Compos. Struct.*, **94** (11), 3132–3141, (2012). <http://dx.doi.org/10.1016/j.compstruct.2012.04.031>
- <sup>24</sup> Chopra, I. Review of state of art of smart structures and integrated systems, *AIAA J.*, **40** (11), 2145–2187, (2002). <http://dx.doi.org/10.2514/2.1561>
- <sup>25</sup> Haddad, Y. Intelligent materials for engineering applications: A review, *AES-ATEMA International Conference Series, Advances and Trends in Engineering Materials and their Applications*, 151–162, (2011).
- <sup>26</sup> Sims, N. D., Stanway, R., and Johnson, A. R. Vibration control using smart fluids: A state-of-the-art review, *Shock Vib. Digest*, **31** (3), 195–205, (1999). <http://dx.doi.org/10.1177/058310249903100302>
- <sup>27</sup> Yalcintas, M., Coulter, J. P., Don, D. L. Structural modeling and optimal Control of electrorheological material based adaptive beams, *Smart Mater. Struct.*, **4** (3), 207–214, (1995). <http://dx.doi.org/10.1088/0964-1726/4/3/008>
- <sup>28</sup> Yeh, J. Y., Chen, L. W., Wang, C. C. Dynamic stability of a sandwich beam with a constrained layer and electrorheological fluid core, *Comput. Struct.*, **64** (1), 47–54, (2004). [http://dx.doi.org/10.1016/S0263-8223\(03\)00212-5](http://dx.doi.org/10.1016/S0263-8223(03)00212-5)
- <sup>29</sup> Yeh, J. Y. and Chen, L. W. Dynamic stability analysis of a rectangular orthotropic sandwich plate with an electrorheological fluid core, *Comput. Struct.*, **72** (1), 33–41, (2006). <http://dx.doi.org/10.1016/j.compstruct.2004.10.010>
- <sup>30</sup> Yeh, J. Y. and Chen, L. W. Finite element dynamic analysis of orthotropic sandwich plates with an electrorheological fluid core layer, *Comput. Struct.*, **78** (3), 368–376, (2007). <http://dx.doi.org/10.1016/j.compstruct.2005.10.010>
- <sup>31</sup> Narayana, V. G. and Ganesan, N. Critical comparison of viscoelastic damping and electrorheological fluid core damping in composite sandwich skew plates, *Comput. Struct.*, (2), 221–233, (2007). <http://dx.doi.org/10.1016/j.compstruct.2006.05.004>
- <sup>32</sup> Rajamohan, V., Sedaghati, R., and Rakheja, S. Optimal vibration control of beams with total and partial MR-fluid treatments, *Smart Mater. Struct.*, **20** (11), (2011). <http://dx.doi.org/10.1088/0964-1726/20/11/115016>
- <sup>33</sup> Choi, S. B., Seo, J. W., Kim, J. H., and Kim, K. S. Electrorheological fluid-based plate for noise reduction in a cabin: experimental results, *J. Sound Vib.*, **239** (1), 178–185, (2001). <http://dx.doi.org/10.1006/jsvi.2000.3051>
- <sup>34</sup> Szary, M. L. The phenomena of electrorheological fluid behavior between two barriers under alternative voltage, *Arch. Acoust.*, **29** (2), 243–258, (2004).
- <sup>35</sup> Lu, H., Meng, G., and Zhang, T. Dynamic and acoustic characteristics high frequency region for sandwich cylindrical cavity embedded with ER fluid, *J. Vib. Eng.*, **17** (4), 457–461, (2004).
- <sup>36</sup> Tang, H., Luo, C., and Zhao, X. Sonic resonance in a sandwiched electrorheological panel, *J. Appl. Phys.*, **98** (1), (2005). <http://dx.doi.org/10.1063/1.1941466>
- <sup>37</sup> Hasheminejad, S. M. and Shabanimotlagh, M. Magnetic-field-dependent sound transmission properties of magnetorheological elastomer-based adaptive panels, *Smart Mater. Struct.*, **19** (3), (2010). <http://dx.doi.org/10.1088/0964-1726/19/3/035006>
- <sup>38</sup> Hasheminejad, S. M. and Maleki, M. Free vibration and forced harmonic response of an electrorheological fluid-filled sandwich plate, *Smart Mater. Struct.*, **18** (5), (2009). <http://dx.doi.org/10.1088/0964-1726/18/5/055013>
- <sup>39</sup> Leissa, A. W. *Vibration of Plates*, (1969), NASA SP-160, NASA, Washington, D.C. Reprinted by the Acoustical Society of America, Woodbury, NY, (1993).
- <sup>40</sup> Rayleigh, L. *The Theory of Sound*, Macmillan, London, (1896).
- <sup>41</sup> Kinsley, L. E. and Frey, A. R. *Fundamentals of Acoustics*, John Wiley & Sons, Inc., New York, (1962).
- <sup>42</sup> Kang, H. J., Ih, J. G., Kim, J. S., and Kim, H. S. Prediction of sound transmission loss through multilayered panels by using Gaussian distribution of directional incident energy, *J. Acoust. Soc. Am.*, **107** (3), 1413–1420, (2000). <http://dx.doi.org/10.1121/1.428428>
- <sup>43</sup> Fahy, F. J. *Foundations of Engineering Acoustics*, UK: Academic, 2001.
- <sup>44</sup> Pellicier, A. and Trompette, N. A review of analytical methods, based on the wave approach, to compute partitions transmission loss, *Appl. Acoust.*, **68** (10), 1192–1212, (2007). <http://dx.doi.org/10.1016/j.apacoust.2006.06.010>
- <sup>45</sup> Yalcintas, M. and Coulter, J. P. Electrorheological material based adaptive beams subjected to various boundary conditions, *J. Intel. Mat. Syst. Str.*, **6** (5), 700–717, (1995). <http://dx.doi.org/10.1177/1045389X9500600511>
- <sup>46</sup> Yeh, J. Y. and Chen, L. W. Vibration of a sandwich plate with a constrained layer and electrorheological fluid core, *Compos. Struct.*, **65** (2), 251–258, (2004). <http://dx.doi.org/10.1016/j.compstruct.2003.11.004>
- <sup>47</sup> Sakuma, T. and Oshima, T. Numerical vibro-acoustic analysis of sound insulation performance of wall members based on a 3-D transmission model with a membrane/plate, *Acoust. Sci. Tech.*, **22** (5), 367–369, (2001). <http://dx.doi.org/10.1250/ast.22.367>
- <sup>48</sup> Tewes, S. Active trim panel attachments for control of sound transmission through aircraft structures, PhD diss., Institute of Lightweight Structures, Technische Universitt Mnchen, Germany, (2005).
- <sup>49</sup> Schiller, N. and Beck, B. Numerical study of transmission loss through a slow gas layer adjacent to a plate, *NASA Technical Report No. NF1676L-16143*, (2013).